RSC Advances

PAPER

View Article Online
View Journal | View Issue

Cite this: *RSC Adv.*, 2023, **13**, 25334

Decoration of polystyrene with nanoparticles of cobalt hydroxide as new composites for the removal of Fe(III) and methylene blue from industrial wastewater

Marzouk Adel,[a] Ahmed M. A. El Naggar,[*b] Ahmed Bakry,[c] Maher H. Hilal,[c] Adel A. El-Zahhar,[d] Mohamed H. Taha[e] and A. Marey[f]

Effluent water from different industries is considered one of the most serious environmental pollutants due to its non-safe disposal. Therefore, proper treatment methods for such wastewater are strongly stimulated for its potential reuse in industries or agriculture. This study introduces a composite fabricated *via* doping of polystyrene with nanoparticles of cobalt hydroxide as a novel adsorbent for dye and heavy metal decontamination from wastewater. The adsorbent fabrication involves the preparation of polystyrene *via* high-internal phase emulation (HIPE) polymerization followed by its intercalation with particles of alkali cobalt. The chemical composition and structural properties of the synthesized composite were confirmed by X-ray diffraction (XRD), Fourier transform infrared (FTIR) spectroscopy, and energy-dispersive X-ray spectroscopy (EDX). Moreover, scanning electron microscopy (SEM) and N_2 adsorption–desorption surface area analysis were performed to identify the surface and morphological characteristics of the composite. Then, the ability of this structure toward the removal of methylene blue dye (MB) and heavy metal (iron III) species from waste aqueous solutions was investigated. Successful elimination for both MB and Fe(III) was achieved by the presented composite. Elevated adsorption capacities of 75.2 and 112.3 mg g^{-1}, toward MB and Fe(III) respectively, were detected for the presented polymer-metal hydroxide composite. The increased values of the composite are attributed to the presence of both organic and inorganic functional groups within its structure. Kinetic and isotherm studies for the removal of both cationic species revealed that adsorption processes fit the pseudo-second-order kinetic model and Langmuir isotherm model. Additionally, thermodynamics measurements indicated that the adsorption process of methylene blue and Fe ions is feasible, spontaneous, physisorption, and endothermic.

Received 6th June 2023
Accepted 31st July 2023

DOI: 10.1039/d3ra03794k

rsc.li/rsc-advances

1 Introduction

The growing industrial, agricultural, and regional activities across the world have resulted in the release of huge amounts of wastewater. Three main categories of contaminants, namely, microorganisms, organics, and inorganics exist in wastewater.[1,2] Dyes and metal ions respectively represent the major organic and inorganic pollutants in water samples. These contaminants have been paid much attention because of their toxicities to ecological and biological systems.[3,4] Metals such as iron, cadmium and lead are counted as the most common inorganic pollutants since they are generated from many industries including fertilizer industries, metal plating, mining operations, paper industries and pesticides.[5,6] Furthermore, organic contaminants of dyes such as methylene blue, reactive dyes and methyl orange are of wide availability in the samples of effluent water from pharmaceutical, cosmetic, leather, textile, plastic and paper industries.[7–9] Special concerns have arisen from these pollutants due to the ability of organisms to store, accumulate and transfer them. Therefore, these may cause serious public health problems in several animals and human beings.[2–5] Accordingly, wastewater systems have become serious problems that need to be urgently solved.

Enormous efforts and several research studies have reported the remediation of water pollution caused by species such as dyes and metal ions. Various techniques including reverse osmosis,[10] flocculation,[11] electrochemical precipitation,[12] ion

[a]*Aluminum Sulphate Company of Egypt, Egypt*
[b]*Egyptian Petroleum Research Institute (EPRI), Nasr City, Cairo, Egypt. E-mail: drmeto1979@yahoo.com*
[c]*Chemistry Departments, Faculty of Science, Helwan University, Cairo, Egypt*
[d]*Department of Chemistry, Faculty of Science, King Khalid University, Abha 9004, Saudi Arabia*
[e]*Nuclear Materials Authority, P.O. Box 530, El Maddi, Cairo, Egypt*
[f]*Department of Basic Science, The Valley Higher Institute for Engineering & Technology, Al-Obour 11828, Egypt*

exchange[13] and adsorption[14–16] have been developed and utilized to circumvent water pollution. Among these techniques, adsorption has been extensively used to remove metal ions and dyes from wastewater samples since it offers process simplicity, low operating costs and high efficiency.[17–21] Efficient adsorbents for such removals may include zeolites, polymers, bio-carbon materials, metal oxides and clays.[1–5]

Of these structures, polymers are characterized by many good features including tolerability, good mechanical properties and low fabrication costs. Therefore, they are widely employed in many applications such as packaging, tissue engineering, drug delivery and wastewater remediation.[22,23] Polymer composites can offer superior properties to individual polymers in some specific applications such as transportation, marine, aerospace/defense, electromagnetic shielding and wastewater treatment.[24,25] The adsorption efficiency of polymer composites toward the present pollutants in wastewater samples has been extensively studied over the past few decades.[26,27] Among these composites, metal–organic framework/poly-dopamine[28] and clay-based composites[29] are found to exhibit enhanced absorptivity toward water contaminants. Furthermore, inorganic structures such as metal oxides and hydroxides offer unique physical and chemical properties such as large specific surface areas and abundant active sites. Hence, they have been applied in many applications including catalysis and water treatment.[30] However, their high surface-to-volume ratio increases the tendency of their particles to aggregate together. Thus, combining metal oxides or hydroxides with polymers or metal organic framework structures produces hybrid organic/inorganic materials through which the aggregation of particles can be avoided. Additionally, these composites may exhibit properties that are not presented by their composing materials separately.[22–24]

Polystyrene-activated carbon composites were used effectively for the removal of methyl orange as an organic pollutant from wastewater.[31] A novel hybrid nanomaterial was fabricated by encapsulating ZrO_2 nanoparticles into spherical polystyrene beads (MPS) covalently bound with charged sulfonate groups ($-SO^{3-}$) and applied for the removal of Pb(II) from wastewater.[32] A polystyrene/AlOOH hybrid material has been prepared by a sol–gel method and applied for Pb(II) decontamination from wastewater.[33] Polystyrene/CuO/calcined layered double hydroxide (PS/CuO@CLDH) microspheres were successfully fabricated by the dispersion polymerization method and applied for the efficient removal of Congo red (CR) from wastewater.[34] A poly(styrene-*block*-acrylic acid) di-*block* copolymer/Fe_3O_4 magnetic nanocomposite (abbreviated as P(St-*b*-AAc)/Fe_3O_4) was prepared by a reversible addition fragmentation transfer (RAFT) method and applied for the removal of antibiotic compounds from wastewater.[35] A calcium–barium phosphate (CBP) composite membrane with 25% polystyrene was prepared by a co-precipitation method and utilized for the efficient desalination of saline water and more importantly demineralization process.[36] Titanium dioxide nanowires (TiO_2-NWs) were successfully prepared by a hydrothermal method and then embraced in polystyrene (PS) to form nanocomposites *via* emulsion polymerization of styrene monomers in the presence of different ratios of TiO_2 nanowires. The prepared polystyrene/TiO_2-NW nanocomposite material was applied for the removal of organochlorine pesticide (OCPs) residues from contaminated water.[37]

In agreement with the trend of wastewater purification *via* adsorption, this study introduces a composite made up of cobalt hydroxide and polystyrene as a novel structure for the removal of methylene blue dye and iron species from waste aqueous solutions. The novelty of this research work is based on presenting a composite adsorbent for the removal of heavy metals and dyes, with a different composition (PS–$Co(OH)_2$) than those previously reported in the literature, which are generally based on carbon structures, functionalized polymers and metal oxides (or mixed-metal oxides). Moreover, the introduced composite in this study relies on the presence of OH anions to interact with cationic species as well as the presence of cobalt (cation), which can have affinity to anionic species and heavy metals too. Therefore, this composite shows tendency and effective selectivity toward several species simultaneously, unlike other presented adsorbents in previous studies, which mostly have selectivity toward a certain substance. In addition, the presence of OH groups can facilitate extra adsorption mechanisms *via* hydrogen bonding and anion exchange; thus, several adsorption mechanisms can potentially take place, at the same time, by PS–$Co(OH)_2$. Furthermore, the use of PS with highly porous nature as support to Co nanoparticles could help in their high dispersion, leading to good enhancement for the adsorption performance of the introduced composite in this research work. The adsorption efficiency of this composite, under the effect of different operational parameters, was investigated. Moreover, the kinetics and thermodynamics of the introduced adsorption processes were also studied.

2 Experimental

2.1. Materials

Styrene, potassium per sulfate, sodium dodecyl sulfate, ferric chloride, and methylene blue dye (MB) were purchased from Sigma-Aldrich Co. (St Louis, MO, USA). The prior-stated reagents were used as received with no further treatments. Different industrial wastewater samples containing Fe^{3+} (100 mg L^{-1}) for sample (1), and MB dye (40 mg L^{-1}) for sample (2) were collected from iron foundries in El Obour city and textile company in Abu Zaabal, Egypt respectively (Table 1).

2.2. Preparation of PS

Polystyrene was synthesized *via* a high-internal phase emulsion polymerization technique. Experimentally, styrene (4.96 g) was mixed with sodium dodecyl sulfate (0.494 g), as a surfactant, producing the oil phase for PS synthesis. The mixture was then added to 11 mL of deionized water at 60 °C under stirring, forming an emulsion. Potassium per sulfate (0.23 g) was then added to the mixture, as an initiator, to allow polymerization to occur. The mixture was kept under stirring for 2 h at 60 °C. Subsequently, the emulsion was dried in an oven at 60 °C for 12 h to get the PS polymer ready and fully synthesized.[22]

Table 1 CAS registry numbers and source of the chemicals

	Formula	CAS number	Assay	Supplier
Industrial wastewater sample (1); contains Fe^{3+} (100 mg L^{-1})	N/A	N/A	N/A	Textile companies in El Obour city, Egypt
Industrial wastewater sample (2); MB dye (40 mg L^{-1})	N/A	N/A	N/A	Iron foundries in Abu Zaabal, Egypt
Styrene	$C_6H_5CH{=}CH_2$	100-42-5	≥99.0%	Sigma-Aldrich Co. (St Louis, MO, USA)
Potassium per sulfate	$K_2S_2O_8$	7727-21-1	≥99.0%	
Sodium dodecyl sulfate	$CH_3(CH_2)_{11}OSO_3Na$	151-21-3	≥98.5%	
Ferric chloride	$FeCl_3$	7705-08-0	97%	
Methylene blue dye	$C_{16}H_{18}ClN_3S{\cdot}3H_2O$	122965-43-9	N/A	

2.3. Preparation of $Co(OH)_2$/PS composites

An aqueous solution of $CoCl_2$ was prepared (1.3 g in 100 mL deionized water) and kept under vigorous stirring at 80 °C until the solution became clear. Promptly, PS (1.4 g) was subsequently added to the solution where stirring was continued for 15 min. Next, NaOH (0.1 M) was drop-wise added under stirring till complete precipitation of cobalt hydroxide (pH of 10–11) on PS had taken place. The cobalt hydroxide–loaded PS ($Co(OH)_2$/PS) was filtered and washed several times with deionized water and then dried, in an oven, at 60 °C for 2 h.[22]

2.4. Characterization of $Co(OH)_2$/PS composites

The verification of the structural characteristics of the prepared powder polymers and composite was done by Fourier-transform infrared (FTIR) spectroscopy using a PerkinElmer Spectrometer 400 (PerkinElmer Inc., Waltham, MA, USA) equipped with a Golden Gate diamond single-reflection device. The surface morphology of the produced composite was acquired using a scanning electron microscope (SEM), model QUANTA FEG 250, USA. This microscope has an accelerating voltage of 30 kV and the magnification range between 14 and 1 000 000 times with a high resolution of 1 nm. The SEM device was equipped with an energy-dispersive X-ray (EDX) unit to facilitate the quantitative elemental analysis of samples. X-ray diffraction patterns for the samples were obtained using a Panalytical Diffractometer (X'Pert Pro, USA). The specific surface area of the composite was measured by N_2 adsorption–desorption technique using a Quantachrome TouchWin™, version 1.21, instrument. The surface characteristics measurements were carried out at 77.35 K preceded by sample degassing under vacuum at 60 °C for 6 h.

2.5. Adsorption experiments

The sorption characteristics of the prepared $Co(OH)_2$/PS composites towards methylene blue and Fe(III) ions were studied in batch experiments at room temperature (25 ± 1 °C) using a thermo shaker water bath (scientific precision SWB 27 – 27 L) in polypropylene tubes. The solution pH was adjusted during the sorption process with 0.5 M HCl and 0.5 M NaOH. The equilibrium studies were performed using different metal ion concentrations (10–100 mg MB L^{-1} and 40–200 mg Fe(III) L^{-1}). The sorption kinetics was studied at different reaction time periods (10–300 min). Briefly, a definite amount of the sorbent (m, g) was shaken with a definite volume of the wastewater solution (V, L) containing an initial concentration of 100 mg Fe(III) L^{-1} for sample (1), and 40 mg MB L^{-1} for sample (2). All tests were conducted three times and only a relative error mean value of ≤4% was accepted. After each experiment of adsorption, the spent sorbent was removed from the solution of decontaminated water by filtration using a membrane of pore diameter equal 0.45 μm.

The concentration of the MB solution was determined using a UV-visible spectrophotometer (Jasco V-550, Japan) at 663 nm based on a calibration curve that was previously constructed through utilizing various solutions of MB with known initial concentrations.[8] The concentration of iron in the aqueous solution was determined utilizing the Egyptian Standard method 1700/1989 as follows. Particularly, each tube of measuring included 2.5 mL of hydrochloric acid, which was then supplemented with up to 25 mL distilled water. A drop of $KMnO_4$ was then added to obtain a pink-colored solution. Next, 5 mL KSCN (20%) was added, where the volumes were made up to 50 mL with distilled water. Then, these solutions were measured using a spectrophotometer at a wavelength of 520 nm.[38] The sorption efficiency%, sorption capacity q_e (mg g^{-1}), and the dimensionless distribution constant (K_C) were calculated using the following equations:[17]

$$R\% = \frac{(C_o - C_e)}{C_o} \times 100 \quad (1)$$

$$q_e = (C_o - C_e) \times \frac{v}{m} \quad (2)$$

$$K_C = \left(\frac{q_e}{C_e}\right) \times 1000 \quad (3)$$

3 Result and discussion

3.1. FT-IR analysis of the synthesized polystyrene

The structural characteristics of polystyrene were verified by FTIR analysis (Fig. 1). It can be noticed that the absorption peaks are located along a wide range of wavenumbers in the displayed spectrum.

The first peak at 3026 cm^{-1} was assigned to the aromatic C–H stretching vibration, while the second peak assigned to aliphatic C–H stretching was seen at 2917 cm^{-1}. The next three peaks located at 1596, 1485 and 1451 cm^{-1} respectively were ascribed to the aromatic C–C stretching vibration. The noted peaks at 1233,

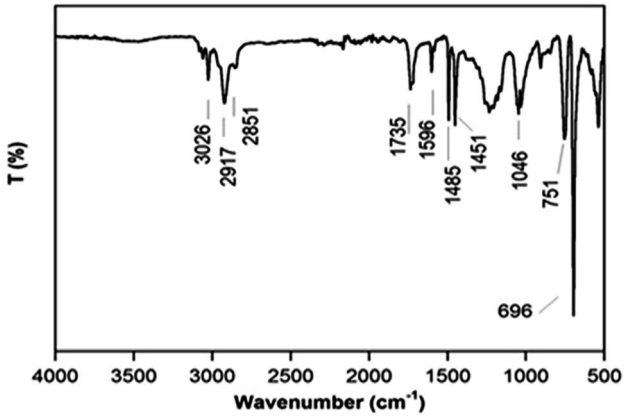

Fig. 1 FT-IR analysis of polystyrene.

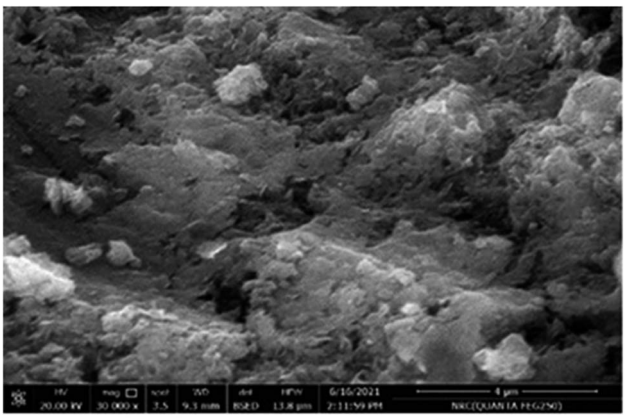

Fig. 2 SEM image of the $Co(OH)_2$/PS composite.

1046, 751, and 695 cm^{-1} were attributed to the vibrational aromatic C–H deformation. The exhibited functional groups in the tested sample qualitatively confirm the successful synthesis of polystyrene.[39]

3.2. Characterization of the prepared $Co(OH)_2$/PS composite

The elemental analysis, morphological structural and surface characteristics of the prepared cobalt hydroxide–polystyrene were studied respectively by energy-dispersive X-ray (EDX), SEM, XRD, FTİR and N_2 adsorption–desorption BET analyses. The morphology of the $Co(OH)_2$/PS composite is illustrated by the SEM images shown in Fig. 2. A highly rough and bit wavy surface could be detected for the obtained composite, which is due to the amorphous nature of polystyrene. However, the surface of proper uniformity with the clear observation of distributed $Co(OH)_2$ particles on the surface of PS could be seen.

The metal hydroxide particles tended to distribute in a good manner throughout the surface of PS. Furthermore, the provided data through the EDX spectrum (Fig. 3) revealed the detection of both Co and O in the as-prepared composite, which is explained due to the successful incorporation of metal hydroxide particles with polystyrene structures. The quantitative Co weight percent, as given by EDX, was found to be 6.9 wt%, which perfectly agrees with the calculated element weight during the preparation stage. This percentage indicates the existence of proper amounts of Co on the surface of the polymer, which is in agreement with the exhibited morphology of $Co(OH)_2$/PS composites through the SEM image. Simultaneously, a high percentage of the C element was noticed through the elemental analysis that are attributed to the polystyrene structure of quite high molecular weight.

The structural characteristic of the composite was acquired by both FTIR and XRD analyses, as respectively shown in Fig. 4 and 5. With regard to the exhibited FTIR spectrum, absorption bands similar to those formerly noticed for blank polystyrene could be detected for the investigated composite. Nevertheless, the intensities of these peaks could be reduced and their shapes had been slightly deformed. These changes in FTIR

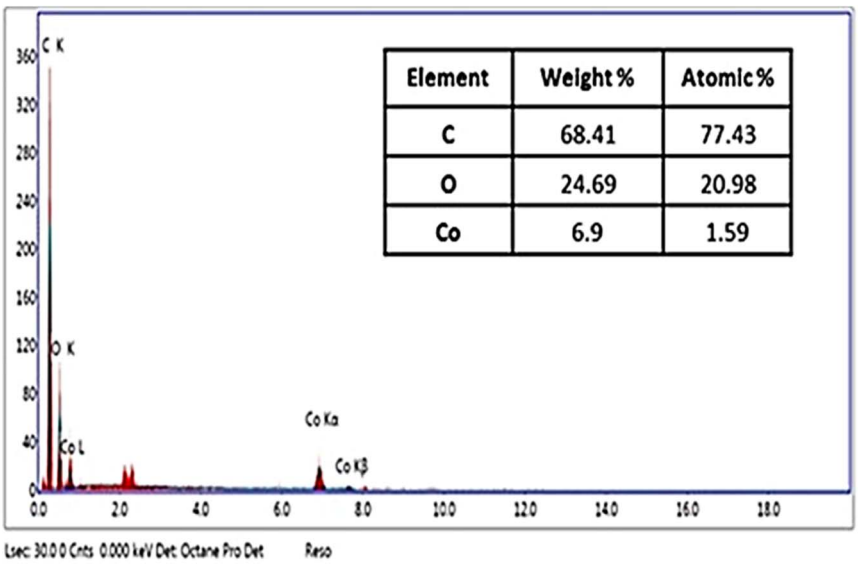

Element	Weight %	Atomic %
C	68.41	77.43
O	24.69	20.98
Co	6.9	1.59

Fig. 3 EDX signals of the $Co(OH)_2$/PS composite.

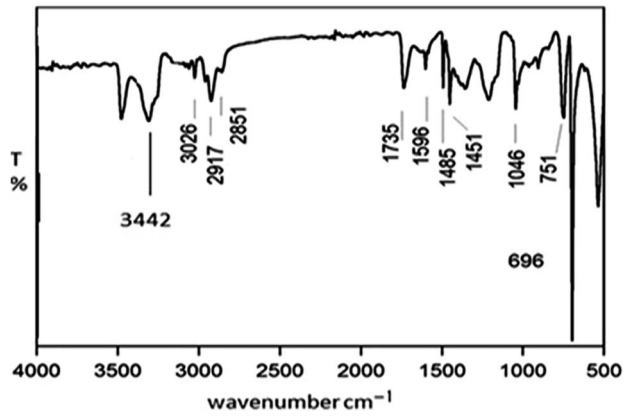

Fig. 4 FTIR spectrum of the $Co(OH)_2$/PS composite.

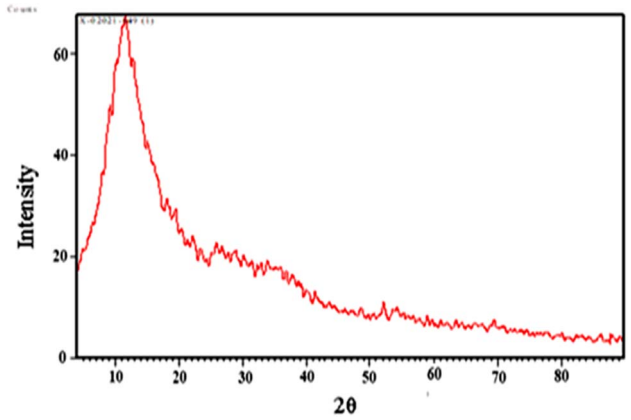

Fig. 5 X-ray diffraction analysis of the $Co(OH)_2$/PS composite.

absorption bands are attributed to the born strain stress in polystyrene particles due to the loading of Co-hydroxide onto their surfaces. Additionally, the presence of hydroxide particles within the structure of the composite was further verified by observing a new intense broad absorption band centered at 3442 cm^{-1}. This FTIR band could be attributed to the stretching vibration mode of –OH, which is present in cobalt hydroxide.

The results of X-ray diffraction (XRD), performed on the $Co(OH)_2$/PS composite, are shown in Fig. 5. The noticed diffraction peak centered at $2\theta = 19.54°$ corresponded to the non-crystalline regions of the composite due to the amorphous nature of polystyrene. The observed diffraction peaks at $2\theta = 32.5°$, 38.5° and 58.97° were assigned to $Co(OH)_2$. These signals are quite sharp with low intensities, which referred to the formation of $Co(OH)_2$ in the shape of crystals; however, they are present with limited number in the composite structure. The displayed XRD pattern could confirm the precipitation of metal hydroxide within the polymer geometry.[40]

The specific surface area of the particles of $Co(OH)_2$/PS composites was determined from the adsorption branch of the N_2 adsorption–desorption isotherm using the Brunauer, Emmett and Teller (BET) eqn (4).

$$\frac{P}{V(P_o - P)} = \frac{1}{V_m C} + \frac{C-1}{V_m C}\frac{P}{P_o} \quad (4)$$

where P_0 is the initial pressure, P is the instant pressure, V is the total volume of gas adsorbed at pressure P, V_m is the volume of monolayer, $C = \exp[(\Delta H_L - \Delta H_1)/RT]$, ΔH_L is the enthalpy of liquefaction and ΔH_1 is the enthalpy of adsorption of the first layer.

Fig. 6 displays the plot of $P/[V(P_0 - P)]$ against P/P_0, as experimentally collected from the N_2 adsorption measurements, where a straight line referring to a correlation coefficient of 0.845 was observed. Thus, the particles of the $Co(OH)_2$/PS composite could exhibit a quite high specific surface area (S_{BET}) value of 186.1 $m^2\ g^{-1}$. This result indicates that the $Co(OH)_2$/PS composite can offer extended adsorption capacity, reflecting its high potential for up-taking the different adsorbates from wastewater samples.

3.3. Sorption investigation

3.3.1. Methylene blue removal using $Co(OH)_2$/PS composites. The sorption tendency of the prepared composite towards methylene blue sorption from industrial wastewater solutions was investigated. The impact of numerous conditions of the sorption capacity such as shaking time, sorbent dose, adsorbate initial concentration, temperature, and solution pH were explored, and the results are presented in Fig. 7.

Fig. 7-I displays the effect of shaking time (10–300 min) on the MB sorption capacity. The attained data declare that the sorption capacity is positively increased as the reaction time increases up to about 150 min (equilibrium state). This could be attributed to the availability of active function groups on the composite surface.[7,8] The maximum sorption capacity was ~33.5 mg g^{-1} at equilibrium. By prolonging the equilibrium time, a steady state was observed. This could be explained based on the surface-active function groups' saturation.[7,8] Fig. 7-II exhibits the variation in sorption capacity as a function of sorbent dose (0.5–3 g L^{-1}). The obtained results indicated that the increase in the sorbent amount of addition is depicted by ramp down in MB sorption capacity, which could be attributed

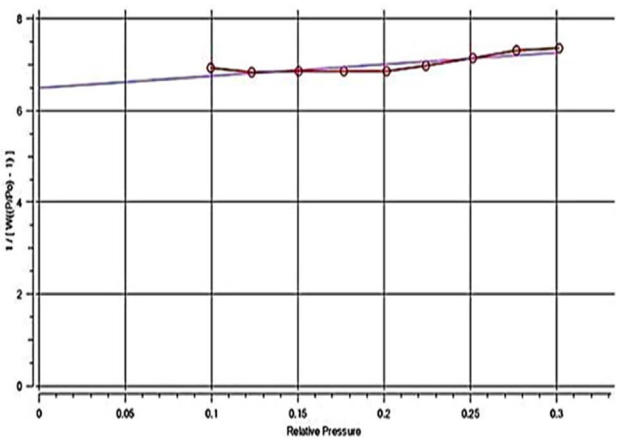

Fig. 6 BET plot of the $Co(OH)_2$/PS composite.

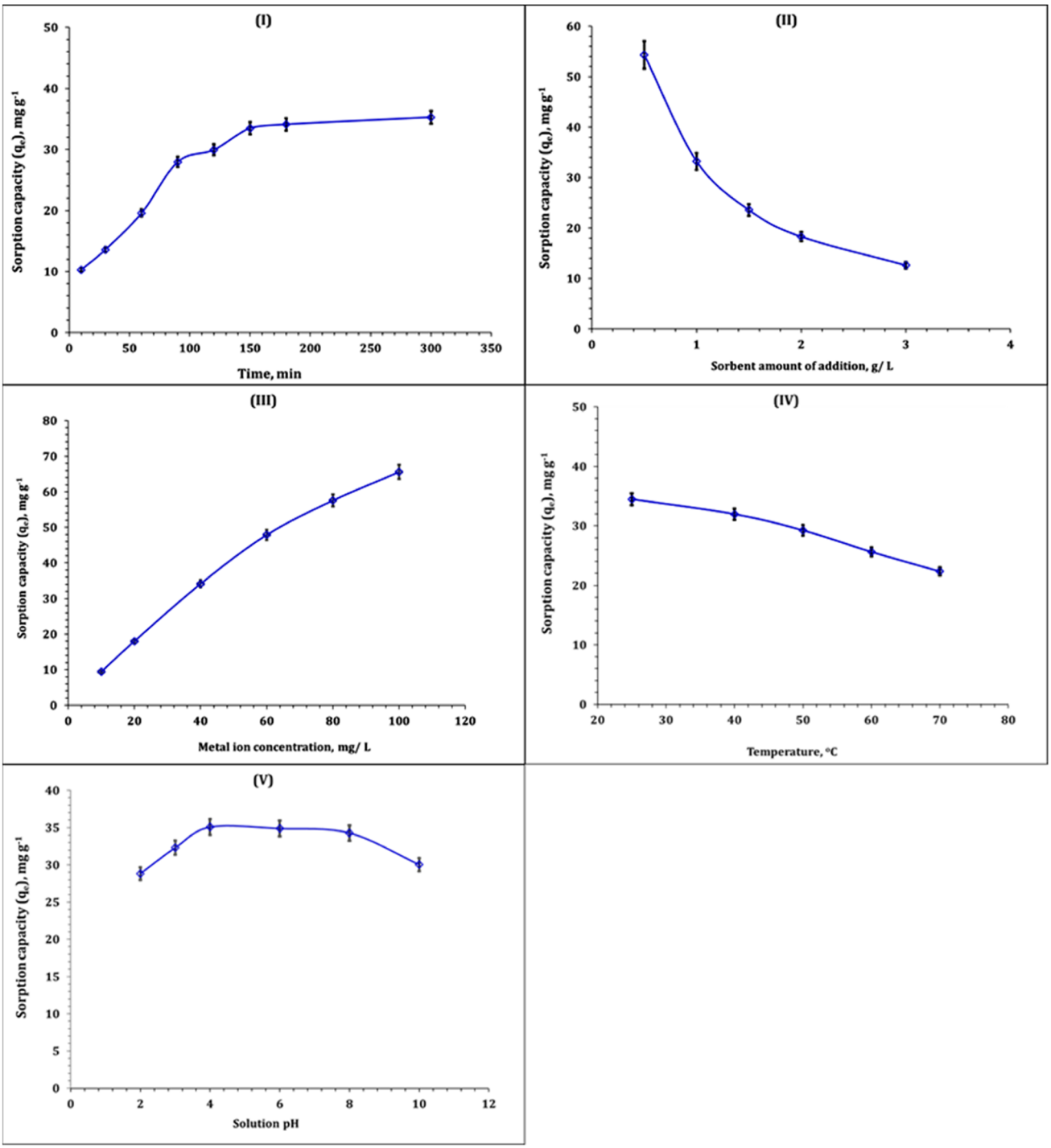

Fig. 7 Effect of different parameters on MB adsorption capacity using $Co(OH)_2$/PS composite: (I) reaction time effect (1.0 g L^{-1}; 150 rpm; pH of 6.5; initial concentration of 40 mg L^{-1}; 25 °C), (II) sorbent dose effect (180 min; 150 rpm; pH of 6.5; initial concentration of 40 mg L^{-1}; 25 °C), (III) initial concentration effect (1.0 g L^{-1}; 180 min; 150 rpm; pH of 6.5; 25 °C), (IV) temperature effect (1.0 g L^{-1}; 150 rpm; pH of 6.5; initial concentration of 40 mg L^{-1}; 180 min), and (V) solution pH effect(1.0 g L^{-1}; 150 rpm; 180 min; initial concentration of 40 mg L^{-1}; 25 °C).

to that the low dye molecule concentration was not equivalent to the available sorbent surface functional groups.[17]

The change in sorption capacity with the variation in MB initial concentration (10–100 mg L^{-1}) is shown in Fig. 7-III. The obtained results explore the increment in the sorption capacity as the adsorbate initial concentration increases. This performance could be due to the availability of active functional groups on the $Co(OH)_2$/PS composite surface for binding to dye molecules.[20,21]

The impact of reaction temperature (25–70 °C) on the MB sorption capacity could be explored from Fig. 7-IV. The exhibited results indicated that the negative influence of the reaction temperature on the sorption capacity reflects the exothermic

nature of the MB sorption process.[20,21] The same exothermic nature has been recognized for MB sorption from wastewater using arginine modified activated carbon,[7] bone char,[14] hydroxyapatite sodium alginate,[20] and thiosemicarbazide-functionalized graphene oxide composite.[21] Fig. 7-V displays the effect of solution pH (2–10) on the MB sorption process. From the Figure, it is clear that the sorption capacity improved as the solution pH increased up to pH 4. The sorption capacity is almost stable at solution pH 4–8. The obtained results are consistent with the literature.[7,20] The increase in solution pH has negative effects on the MB sorption process.

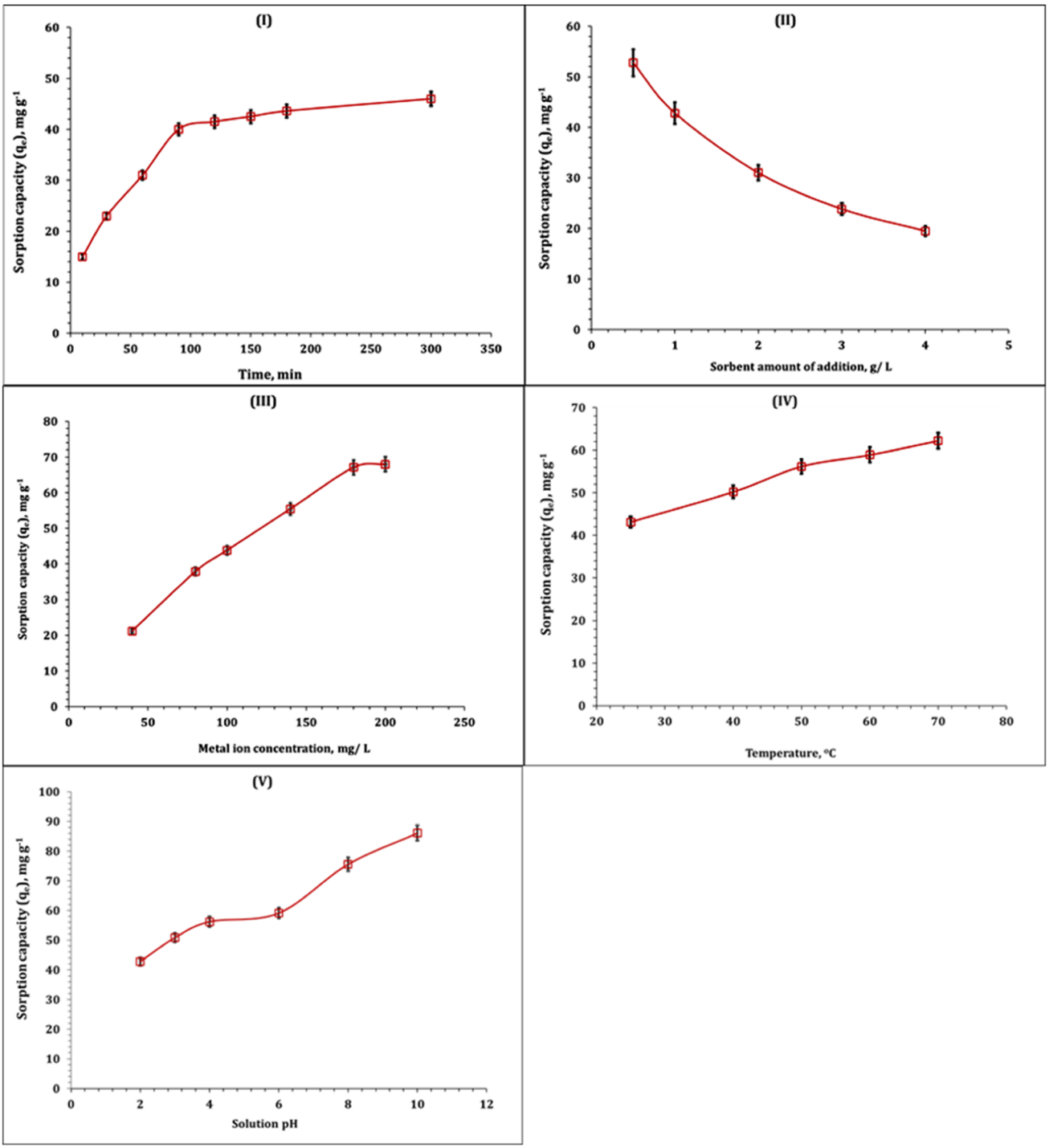

Fig. 8 Effect of different parameters on the Fe(III) adsorption capacity using $Co(OH)_2$/PS composites: (I) reaction time effect (1.0 g L^{-1}; 150 rpm; pH of 2.0; initial concentration of 100 mg L^{-1}; 25 °C), (II) sorbent dose effect (180 min; 150 rpm; pH of 2.0; initial concentration of 100 mg L^{-1}; 25 °C), (III) initial concentration effect (1.0 g L^{-1}; 180 min; 150 rpm; pH of 2.0; 25 °C), (IV) temperature effect (1.0 g L^{-1}; 150 rpm; pH of 2.0; initial concentration of 100 mg L^{-1}; 180 min), and (V) solution pH effect (1.0 g L^{-1}; 150 rpm; 180 min; initial concentration of 100 mg L^{-1}; 25 °C).

3.3.2. Iron(III) ion removal using $Co(OH)_2$/PS composites. Fe(III) removal from industrial wastewater was conducted using $Co(OH)_2$/PS composites. The dependency of the sorption capacity on different reaction conditions such as shaking time, sorbent dose, adsorbate initial concentration, temperature, and solution pH was investigated, and this is shown in Fig. 8.

The dependence of Fe(III) sorption capacity on reaction time (10–300 min) was investigated, and this is explored in Fig. 8-I. The displayed data demonstrate that the Fe(III) sorption capacity is rapidly increasing as the shaking time increases up to 90 min and then reached the steady state. This means that the sorption equilibrium is achieved at 90 min. The maximum sorption capacity at equilibrium is about 40 mg g^{-1}. The rapid increase in the sorption process before equilibrium state is due to the free surface-active sites on the composite; however, after equilibrium, the steady state is achieved due to the occupation of most of the composite active sites.[15,16] Fig. 8-II shows the impact of the composite amount of addition (0.5–4 g L^{-1}) on the Fe(III) sorption capacity. The exhibited results indicated that the sorption capacity is dramatically decreased with the increment in sorbent dose. This performance could be due to that the low dye molecule concentration was not equivalent to the available sorbent surface functional groups.[15–17]

The impact of Fe(III) ion initial concentration (40–200 mg L^{-1}) on the sorption capacity is illustrated in Fig. 8-III. The displayed results indicated the positive impact of the metal ion initial concentration could be due to the availability of active function groups on the $Co(OH)_2$/PS composite surface for binding to Fe(III) ions.[18,19] The variation in Fe(III) ion sorption capacity as a function of reaction temperature (25–70 °C) is explored and presented in Fig. 8-IV. The obtained results indicated that the sorption process is endothermic, whereas the increment in reaction temperature improves the sorption capacity. The same endothermic nature was reported for iron ion sorption from wastewater using chitosan,[15,18] silica-supported organic–inorganic hybrids,[16] and pecan shell-based activated carbon.[19]

Fig. 8-V shows the impact of solution pH (2–10) on the Fe(III) ion sorption process. From the figure, it could be observed that the Fe(III) sorption capacity was low in the acidic medium and tended to increase the pH value 12.0. Iron(III) precipitation was observed at pH 6.0 onwards, and the intensity of precipitation increases with the increase in pH from 6.0 to 10.0, which reflects that the removal may be due to the formation of metal hydroxide precipitation.[15,16]

3.4. Modeling of the sorption process

3.4.1. Sorption kinetic models. The kinetic analysis of experimental data for MB and Fe(III) sorption processes using the $Co(OH)_2$/PS composite was carried out to investigate the mechanism of adsorption, equilibrium time as well as rate controlling steps. In this regard, pseudo-first-order (Lagergren), pseudo-second-order, intra-particle diffusion (Weber–Morris), and Bangham's models were used for analyzing the adsorption results. The linear forms for the applied models are exhibited in eqn (5)–(8) respectively as follows:[41–43]

$$\log(q_e - q_t) = \log q_e - \frac{K_1}{2.303} t \quad (5)$$

$$\left(\frac{t}{q_t}\right) = \frac{1}{K_2 q_e^2} + \frac{1}{q_e} t \quad (6)$$

$$q_t = K_{id} t^{0.5} + C_i \quad (7)$$

$$\log\log\left(\frac{C_o}{C_o - q \times m}\right) = \log\left(\frac{k_o m}{2.303 V}\right) + \alpha \log t \quad (8)$$

where q_e (mg g^{-1}) is the equilibrium concentration of oil molecules and q_t (mg g^{-1}) is the adsorbed amount of oil molecules after time t (min), and k_1 (min^{-1}) and k_2 (min^{-1}) are the rate constants for the pseudo-first and -second orders, respectively. K_{id} (mg g^{-1} $min^{-0.5}$) is a rate constant, C is the thickness of the boundary layer, and K_o and α are constants.

The plot of the Lagergren model was exhibited as the variation in $\log(q_e - q_t)$ as a function of time (Fig. 9-I), the illustration of time/qt against time (Fig. 9-II) represents the pseudo-second-order model, Fig. 9-III displays the relation between q_t and time$^{0.5}$ (Weber and Morris model), while the Bangham plot is displayed by the double logarithmic plot (Fig. 9-IV). The attained values of the kinetic parameters were declared in Table 2.

The values of the kinetic parameters (Table 2) indicate that the pseudo-second-order kinetic model possesses the highest coordination coefficient ($R^2 \geq 0.99$). Besides, the calculated sorption capacities from the pseudo-second order (q_{ecal}) for MB and Fe(III) ions (37.9 and 45.7 mg g^{-1} respectively) are close to the experimental sorption capacity (q_{eexp}) for MB (35.2 mg g^{-1}) and Fe(III) ions (44.4 mg g^{-1}). This means that MB and Fe(III) sorption process using the $Co(OH)_2$/PS composite is fitted well to the pseudo-second order model. This indicates the chemisorption nature for MB and Fe(III) sorption from wastewater, and the removal process involves electron sharing between the composite surface active sites and dye molecules and Fe(III) ions.[41–43] The same kinetic profile was reported for methylene blue and Fe(III) sorption from wastewater using iron-based metal organic frameworks,[8] hydroxyapatite sodium alginate,[20] and thiosemicarbazide-functionalized graphene oxide composites.[21] Moreover, Fe(III) removal from wastewater using chitosan,[15,18] silica-supported organic–inorganic hybrids,[16] and pecan shell-based activated carbon[19] was also obeyed to the pseudo-second-order kinetic model.

The tendency of the prepared composite towards MB and Fe(III) ions could be ranked as follows: Fe(III) ions (44.4 mg g^{-1}) > MB molecules (35.2 mg g^{-1}). Furthermore, the values of the half equilibrium time of MB are higher than those of Fe(III) ions (MB: 1.5 h; Fe(III): 45.6 h), while the initial sorption rate for MB (24.9 mol g^{-1} h^{-1}) is less than that of Fe(III) ions (1.0 mol g^{-1} h^{-1}). This performance confirms that the composite exhibits a higher tendency toward Fe(III) ions than toward MB molecules, and indicates that the equilibrium state for the Fe(III) ion sorption reaction is faster than that of the MB sorption reaction, which is consistent with the experimental results, whereas the equilibrium state for Fe(III) ions is obtained after 90 min, while the MB equilibrium state is reached after 150 min.

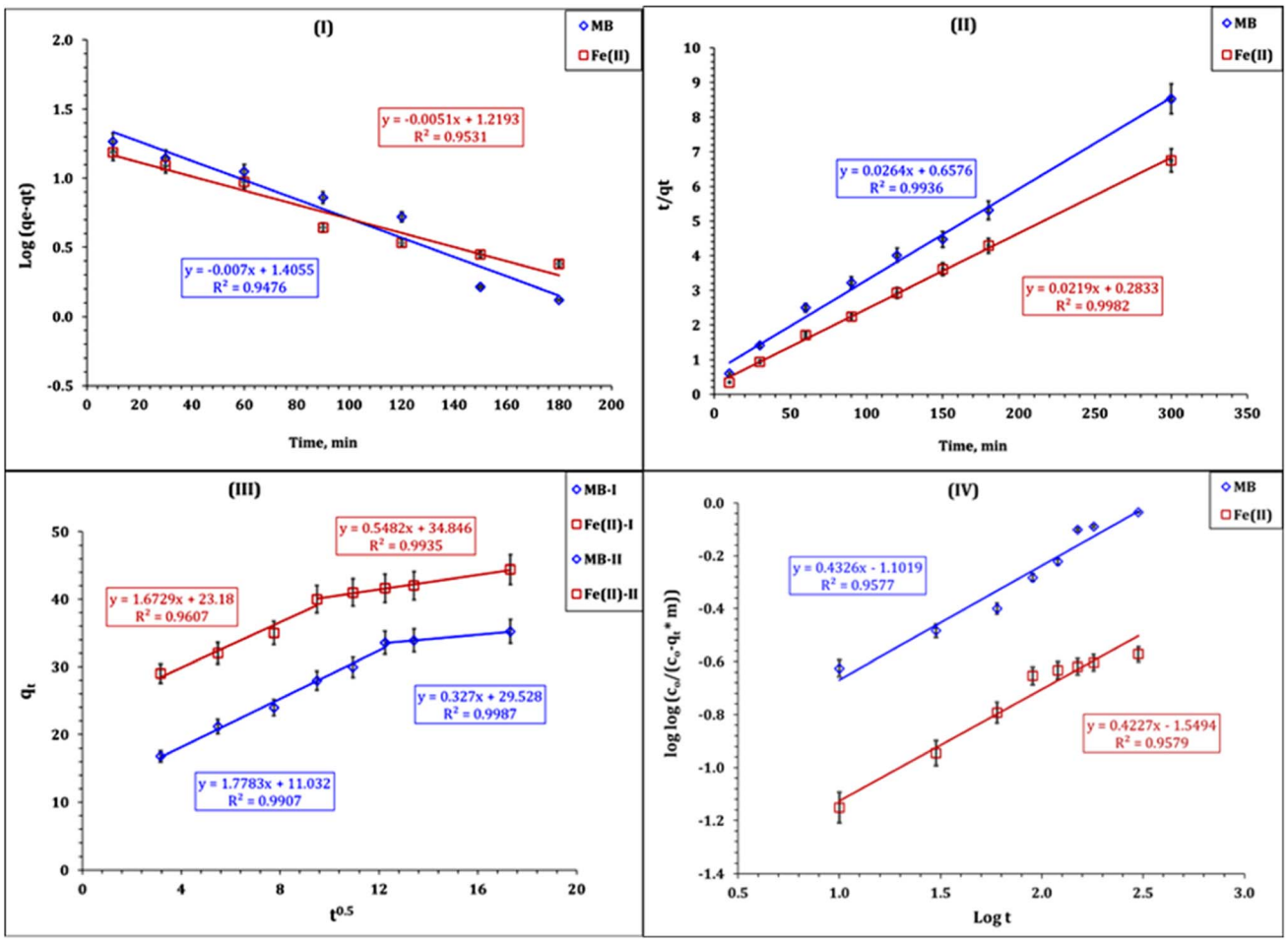

Fig. 9 Illustration of the kinetics of pseudo-first-order (I), pseudo-second-order (II), Weber–Morris (III), and Bangham (IV) models for MB and Fe(III) process.

Table 2 Evaluated parameters of the applied kinetic equations

		MB	Fe(III)
Lagergreen pseudo first-order	k_1 (min^{-1})	0.016	0.012
	q_{ecal} (mg g^{-1})	25.4	16.6
	q_{eexp} (mg g^{-1})	35.2	44.4
	R^2	0.947	0.953
Pseudo second-order	k_2 (min^{-1})	0.001	0.022
	q_{ecal} (mg g^{-1})	37.9	45.7
	q_{eexp} (mg g^{-1})	35.2	44.4
	h (mol g^{-1} h^{-1})	1.52	45.66
	$t_{1/2}$ (h)	24.9	1.0
	R^2	0.993	0.998
Weber and Morris model	Stage I		
	k_i (mg g^{-1} min$^{-1/2}$)	1.78	1.67
	C	11.0	23.2
	R^2	0.991	0.961
	Stage II		
	k_i (mg g^{-1} min$^{-1/2}$)	0.33	0.55
	C	29.5	34.8
	R^2	0.998	0.993
Bangham's equation model	k_o (mg g^{-1} min^{-1})	0.05	0.06
	α	0.67	0.37
	R^2	0.957	0.957

The Weber–Morris kinetic model is applied to explore the mechanism of MB and Fe(III) ion sorption using a $Co(OH)_2$/PS composite. The relation between q_t *versus* time$^{0.5}$ (Weber and Morris plot) displays the mechanisms that control the sorption process, whether it is a solo or multi-reaction mechanism. The sorption process is controlled by a solo reaction mechanism if the plot exhibits a linear relationship passing through the origin; however, it is controlled with multiple mechanism if the plot consists of several segments.[42,43] Fig. 9-III declares that the MB and Fe(III) sorption processes are controlled with multi-reaction mechanisms, whereas the plot consists of two segments. This indicates that the sorption process was performed through two stages; the first stage expresses the sorption process up to reaction equilibrium (150 min for MB and 90 min for Fe(III) ions). This stage was characterized by the rapid rate of reaction, which is due to the availability of free active sites on the composite surface.[41,42] The second stage extends after equilibrium time, and was characterized by the slow rate of reaction, which could be attributed to fill most of the adsorbent surface area holes.[41–43]

It is worth noting that the first stage of Mb and Fe(III) ion sorption processes possess a lower constant C (boundary layer effect) and a higher rate of reaction than the second stage,

reflecting that the sorption process in the first stage occurs at the sorbent surface (high rate of reaction), while in the second stage, the sorption process takes place inside the sorbent pores and the intra-particular diffusion is the controlling mechanism (low rate of reaction).[17,41–43] The same kinetic profile was reported for methylene blue and Fe(III) sorption from wastewater using iron-based metal organic framework,[8] hydroxyapatite sodium alginate,[20] thiosemicarbazide-functionalized graphene oxide composite,[21] chitosan,[15,18] silica-supported organic–inorganic hybrids,[16] and pecan shell-based activated carbon,[19] which also obeyed the pseudo-second-order kinetic model.

The Bangham kinetic plot (Fig. 9-IV) exhibits a good linear relationship ($R^2 \geq 0.95$), which reflects that the MB and Fe(III) ion sorption process is also controlled by the diffusion of adsorbate species into the pores of prepared composites.[41–43] This result is consistent with the findings by Weber–Morris kinetics, whereas the sorption process is controlled with multiple reaction mechanisms.

3.4.2. Sorption isotherm models. The experimental data was analyzed using different conventional isotherm models to explore the isotherm of industrial wastewater treatment using $Co(OH)_2$/PS composites. The applied isotherm models are the Freundlich model, which gives insight into the heterogeneous multilayer adsorption; the Langmuir model assumes with the monolayer adsorption; the Temkin model describes the adsorption heat; and the Dubinin–Radushkevich (D–R) model is related to the adsorption energy.[42–44] Eqn (9)–(12) represent the applied three-isotherm models respectively.[42–44]

$$\frac{C_e}{q_e} = \left(\frac{1}{K_L q_m}\right) + \left[\frac{C_e}{q_m}\right] \quad (9)$$

$$\ln q_e = \ln K_F + \left[\frac{1}{n}\right] \ln C_e \quad (10)$$

$$\ln q_e = \ln q_s + K_{ad}\varepsilon^2 \quad (11)$$

$$q_e = \frac{RT}{b_T} \ln K_T C_e \quad (12)$$

where C_e (mg L^{-1}) is the equilibrium concentration of U(VI) ions, q_{max} (mg g^{-1}) is the theoretical adsorption capacity, K_L is the Langmuir constant, and K_F and n are Freundlich constants. q_s is the theoretical isotherm saturation capacity (mg g^{-1}); K_{ad} is the Dubinin–Radushkevich isotherm constant (mol^2 J^{-2}), and is important to evaluate the mean sorption energy (E_{DR}) which equals $(1/\sqrt{2K_{ad}})$; ε is the Dubinin–Radushkevich isotherm constant and equals $(RT \ln(1 + 1/C_e))$. b_T is the Temkin constant that refers to the adsorption heat and K_T (L min^{-1}) is the equilibrium binding constant.

The variation in ln q_e against ln C_e (Fig. 10-I) was applied to verify the Freundlich isotherm model, the Langmuir model plot (Fig. 10-II) relate C_e/q_e *versus* C_e, Fig. 10-III displays the relation between q_e and ln C_e (Temkin isotherm model), while the relation between ln q_e and ε^2 (D–R model plot) is shown in Fig. 10-IV. The values of the isotherm model parameters are displayed in Table 3. The anticipated results declare that MB and Fe(III) ion sorption processes obeyed the Langmuir isotherm model, but they possess the highest coordination coefficient (R^2 = 0.99). This means that the industrial raffinate effluent treatment using the prepared composite is a homogeneous and monolayer process.[42–44] The same isotherm performance was reported for wastewater treatment using iron-based metal–organic frameworks,[8] hydroxyapatite sodium alginate,[20] thiosemicarbazide-functionalized graphene oxide composites[21] for methylene blue sorption process, and chitosan,[15,18] silica-supported organic–inorganic hybrids,[16] and pecan shell-based activated carbon[19] for the Fe(III) removal process.

Table 3 declares that the $Co(OH)_2$/PS composite exhibits higher sorption tendency for Fe(III) ions (q_m = 112.3 mg g^{-1}) than for MB molecules (q_m = 75.2 mg g^{-1}). The feasibility of MB and Fe(III) sorption processes could be explored from the values of the dimensional constant separation factor (R_L), whereas sorption is feasible if 1 $\langle R_L \rangle$ 0, while it is an unfavorable process if R_L is higher than 1.[17,42–44] Fig. 11 shows that the values of R_L are between 0.3 $\langle R_L \rangle$ 0 for MB, and 0.1 $\langle R_L \rangle$ 0 for Fe(III) ions, which indicates that the sorption process using the $Co(OH)_2$/PS composite is a feasible process.

The Freundlich isotherm model exhibits a proper coordination coefficient (R^2 = 0.98), which reflects that the multilayer sorption process could be present during the MB and Fe(III) ion sorption process.[42–44] In addition, the n values are > 1 (2.05 for MB and 1.65 for Fe(III) ions), indicating the favorable adsorption conditions.[17] The Temkin isotherm model possesses a proper coordination coefficient (R^2 = 0.98), which indicates that this model could also describe well the obtained experimental results. The Temkin isotherm parameters indicated that the heat adsorption of MB and Fe(III) ions are 173.6 and 99.1 J mol^{-1} respectively, and the heat adsorption binding constants of the sorption process are 2.4 and 0.1 L g^{-1} for MB and Fe(III) ions respectively.

The sorption capacity of the applied $Co(OH)_2$/PS composite was compared with other sorbents reported in the literature, and this is shown in Table 4. The applied sorbent shows a relatively fast kinetics, and the equilibrium state is achieved within 240 min. Besides, good removal efficiency at room temperature reflects an energy-efficient process. Finally, the sorption performance and stability of the applied sorbent indicate a promising material for the wastewater treatment approach.

3.4.3. Thermodynamic investigation. The nature of MB and Fe(III) removal from industrial wastewater using $Co(OH)_2$/PS composites could be explored by evaluating the reaction thermodynamic parameters, *i.e.* Gibbs free energy change (ΔG), enthalpy change (ΔH), and entropy change (ΔS). Eqn (13)–(15) declare the applied equations for illustrating the van't Hoff plot (Fig. 12) and evaluating the process thermodynamics variables as follows:[41–43]

$$\log K_C = -\frac{\Delta H^\circ}{2.303R} \times \frac{1}{T} + A \quad (13)$$

$$-\Delta G^\circ = 2.303RT \log K_C \quad (14)$$

$$\Delta G^\circ = \Delta H^\circ - T\Delta S^\circ \quad (15)$$

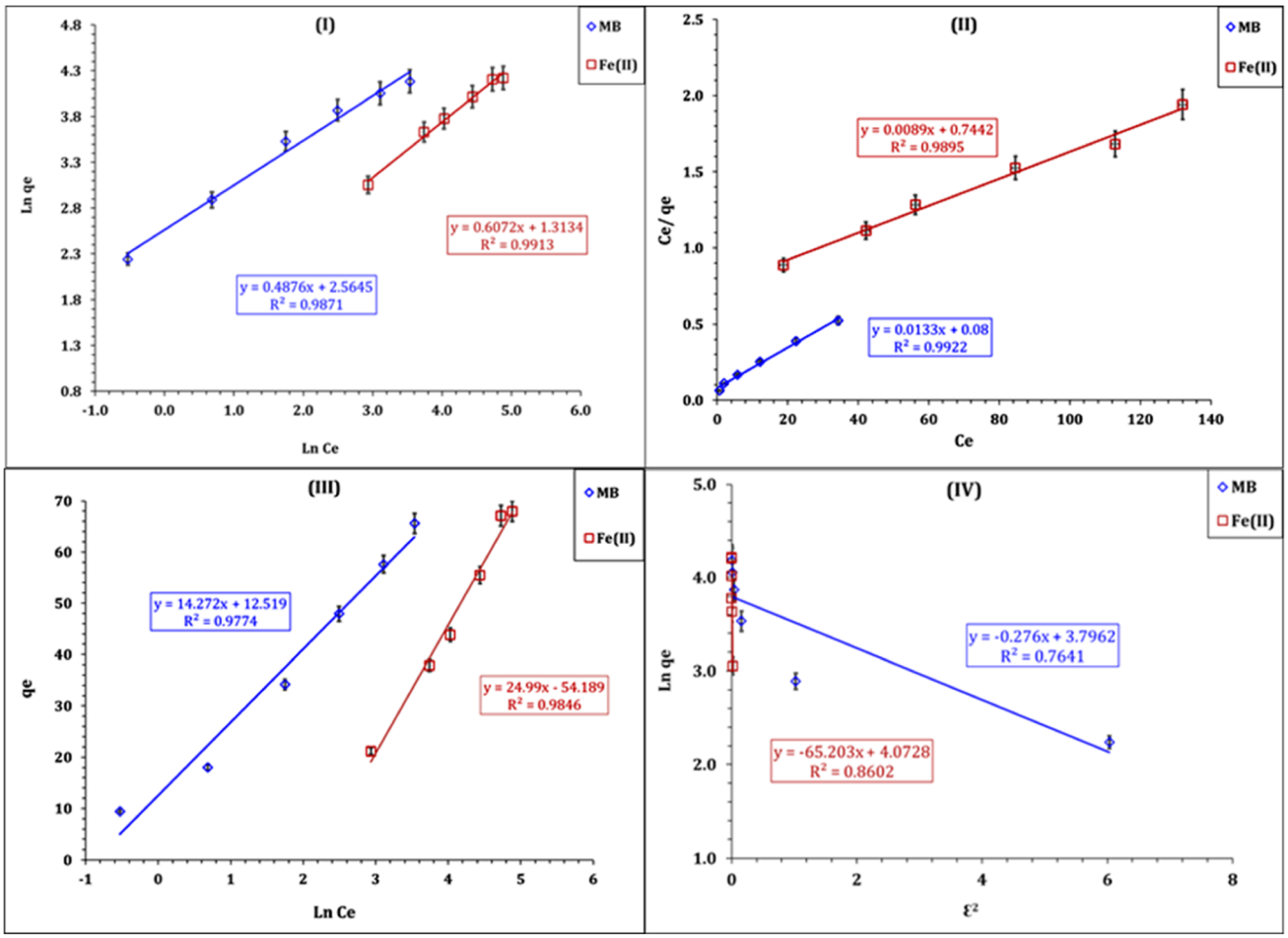

Fig. 10 Illustrate of the isotherm of plots of Freundlich (I), Langmuir (II), Temkin (III), and D–R (IV) models for MB and Fe(III) processes.

Table 3 Evaluated parameters of the applied isotherm equations

		MB	Fe(III)
Freundlich isotherm model	N	2.1	1.6
	K_F (mg g^{-1})	13.0	3.7
	R^2	0.98	0.99
Langmuir isotherm model	q_m (mg g^{-1})	75.2	112.3
	b (L mg^{-1})	0.16	0.97
	R^2	0.99	0.98
R–D isotherm	β (mol^2 kJ^2)	0.61	0.18
	q_m (mmol g^{-1})	9.1	11.7
	E (kJ mol^{-1})	0.9	1.7
	R^2	0.76	0.86
Temkin isotherm	b (J mol^{-1})	173.60	99.14
	B	14.3	25.0
	K_T (L g^{-1})	2.4	0.1
	R^2	0.97	0.98

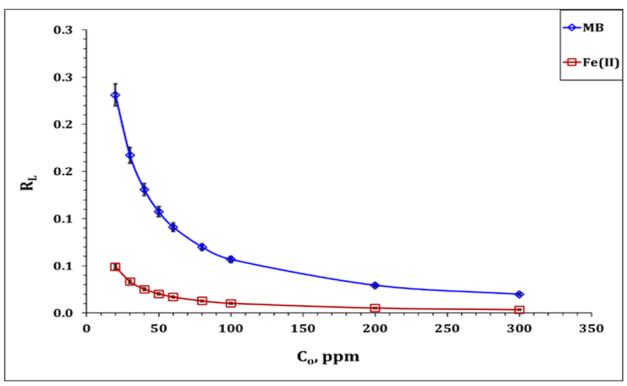

Fig. 11 Separation factor R_L of MB and Fe(III) sorption processes.

where K_C is a non-dimensional equilibrium constant and it equals $K_d \times 1000 \times \rho$;[17] T is the temperature (K), R is the universal gas constant (8.314 J mol^{-1} K^{-1}), ρ is the solution density (g L^{-1}), and A is a constant.

The values of the thermodynamic variables are exhibited in Table 5. The displayed results explore that MB is exothermic in nature, whereas it exhibits a negative ΔH value (−30.6 kJ mol^{-1}). On the contrary, Fe(III) ion sorption is an endothermic process, whereas it possesses a positive ΔH value (14.8 kJ mol^{-1}). The Gibbs free energy change (ΔG) for both MB and Fe(III) ions is negative, which reflects a feasible and spontaneous reaction.[41–43] The MB sorption process is characterized by decreasing the randomness at the solid–solution interface,

Table 4 Comparison of the maximum sorption capacities of different sorbents for MB and Fe(III)

Sorbent type	C_e, mg g^{-1}	Time, min	Temp, °C	pH	q_e, mg g^{-1}	Ref.
MB						
Graphene hybridized polydopamine-kaolin composite	5–40	1440	27	—	39.6	45
Bentonite and opuntiaficusindica	10–360	15	—	6	30.1	11
Mesoporous CuO@BSS nanocomposite	5–100	30	—	10	50.0	46
Magnetic clinoptilolite/chitosan/EDTA	10–50	120	40	5.5	44.4	47
Silica aerogel/Ni/C/N	5–100	30	30	—	115.0	48
Fe_3O_4@C nanocomposite	15–40	720	25	7	52.5	49
Fe-BDC MOF	1–5	1440	—	—	8.6	8
$Co(OH)_2$/PS composite	10–100	180	25	6.5	75.2	P.W.
Fe(III) ions						
Silica-supported organic–inorganic hybrid sorbents	50–700	30	25	5	97.1	16
Pecan shell based activated carbon	25–100	90	30	3	41.6	19
Cross-linked chitosan	3–9	60	—	5	64.1	18
Chitosan	10–50	240	30	4	28.7	15
Rice husk ash	2–40	60	5	25	6.21	50
Chitosan/polyethylene glycol blend membrane	2–10	80	27	5	90.9	51
Activated carbon from coconut shells	20–100	90	25	6	81.8	52
$Co(OH)_2$/PS composite	40–200	180	25	2	112.3	P.W.

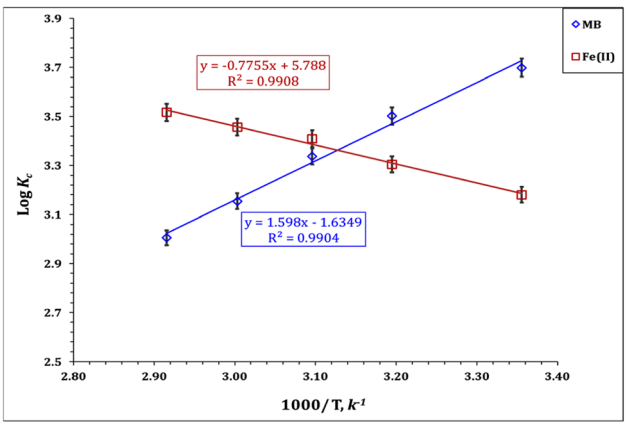

Fig. 12 Van't Hoff plot for MB and Fe(III) ion sorption processes.

whereas it shows a negative ΔS value (−31.9 kJ mol^{-1} K); however, the Fe(III) sorption process exhibits a positive ΔS value (110.7 kJ mol^{-1} K) reflecting an increase in the randomness at the solid–solution interface.[41–43] The same thermodynamic performance (exothermic, spontaneous, and feasible process) was reported for methylene blue sorption from wastewater using iron-based metal organic frameworks,[8] hydroxyapatite sodium alginate,[20] and thiosemicarbazide-functionalized graphene oxide composites.[21] Moreover, Fe(III) removal from wastewater by sorption thermodynamics properties such as endothermic, spontaneous, and feasible processes was reported for wastewater treatment using chitosan,[15,18] silica-supported organic–inorganic hybrids,[16] and pecan shell-based activated carbon.[19]

Table 5 Thermodynamic parameters for MB and Fe(III) ion sorption processes

	ΔG (kJ mol^{-1})					ΔH	ΔS
	25 °C	40 °C	50 °C	60 °C	70 °C	(kJ mol^{-1})	(J mol K^{-1})
MB	−21.1	−21.0	−20.6	−20.1	−19.7	−30.6	−31.9
Fe(III)	−18.1	−19.8	−21.1	−22.0	−23.1	14.8	110.7

3.5. Impact of competing ions

Wastewater solutions contain diverse ions such as Na^+, K^+, Mg^{2+}, Ca^{2+}, and Mn^{2+} along with the organic dye molecules.[39,55] The assessment of the practical application of $Co(OH)_2$/PS for the treatment of wastewater solutions generated from textile industries and iron foundries was achieved by investigating the impact of coexisting metal ions on the sorption performance of

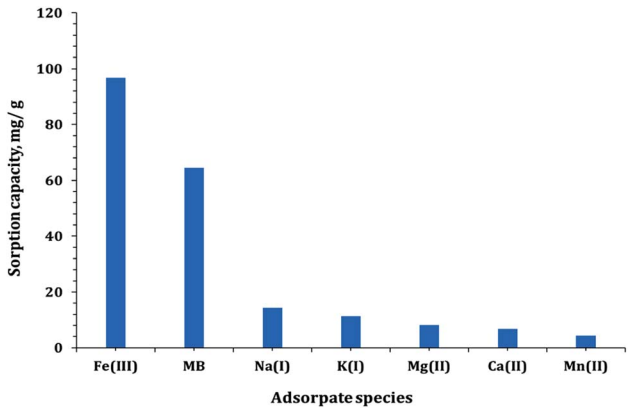

Fig. 13 Effect of the coexisting ions on the sorption capacity of Mb and Fe(III).

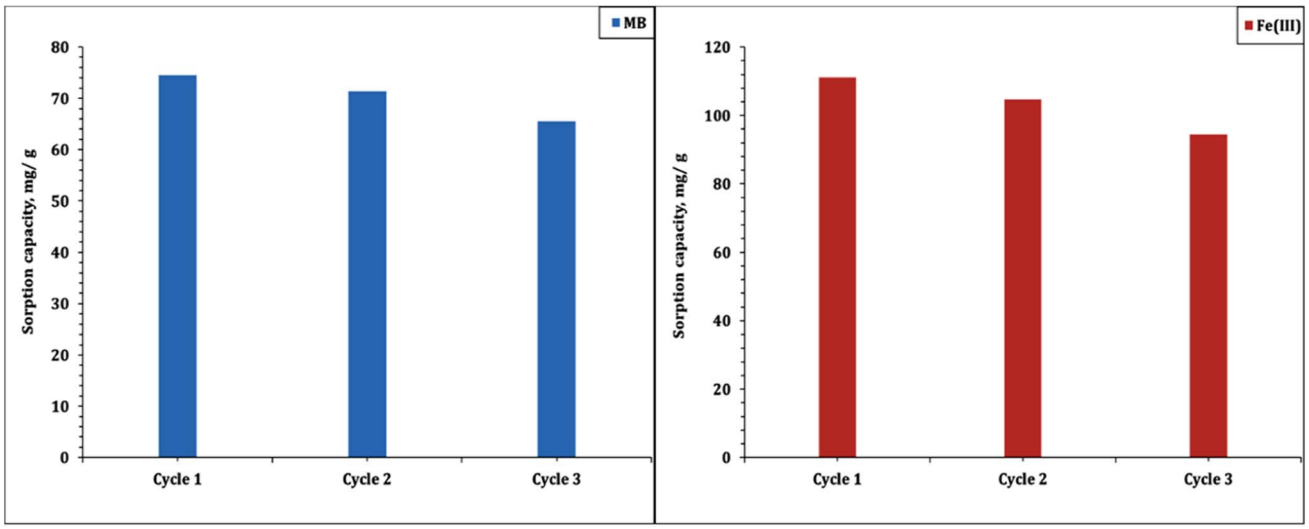

Fig. 14 Recyclability of the $Co(OH)_2$/PS composite.

$Co(OH)_2$/PS. In this regard, the impact of a mixed solution of Na^+, K^+, Mg^{2+}, Ca^{2+}, and Mn^{2+} with an initial concentration of 50 mg L^{-1} of each metal ion on the adsorption capacity of MB and Fe(III) was investigated. The attained results in Fig. 13 indicate that the sorption capacity of MB and Fe(III) was reduced by about 14 and 18% from the sorption capacity without the interfering ions. Nevertheless, the prepared $Co(OH)_2$/PS composite exhibits higher sorption capacities for Fe(III) and MB in comparison with other interfering ions. This indicates that the prepared composite exhibits a proper potentiality for the application in wastewater treatment approaches.

3.6. Reusability investigation

The sorbent reusability is an important parameter in terms of sustainable process. In this regard, the spent $Co(OH)_2$/PS composite was washed with distilled water and then introduced to the elution process using a hydrochloric acid solution.[7,53,54] The stability of the prepared $Co(OH)_2$/PS composite for three consecutive sorption/desorption cycles was investigated, and the results are displayed in Fig. 14. The anticipated data declare that the sorption capacity of MB and Fe(III) decreased by about 12 and 15% respectively from the sorption capacity of the fresh sorbent, which reflects good stability for the prepared composite and potentiality for application as a sorbent in environmental clean-up processes.

4 Conclusion

In this research, a $Co(OH)_2$/PS composite has been prepared and tested as a new adsorbent for the removal of cationic species contaminants including methylene blue dye and Fe(III) from wastewater samples. XRD, FT-IR and EDX analyses confirmed the structural characteristics of the introduced composite. Additionally, measurements of surface properties indicated the high specific surface area of this composite. Moreover, good uniform morphological features could be presented by the composite. Adsorption studies showed that the contact time, composite dose and temperature positively increased the removal efficiency of MB and Fe(III) by the composite. By applying kinetic and isotherm models on the experimental data of adsorption, it was noted that the process followed the pseudo-second-order kinetic model and Langmuir isotherm model. The thermodynamics studies revealed that the adsorption was endothermic; however, it was spontaneous and feasible (ΔG exhibited negative values). This means that the adsorption was driven by entropy change rather than enthalpy change.

Data availability

There is a ESI File is provided with this submission. However, any other data will be available upon request.

Author contributions

MrMarzouk Adel: performing the experimental work and the materials analysis. Dr Ahmed El Naggar: supervising the synthesis of materials and writing the manuscript. Dr Ahmed Bakry: supervising the experimental work. Professor Maher Hilal: contributed in preparing the manuscript. Dr Adel El-Zahhar: contributing in data interpretation and revising the article. Dr Mohamed Taha: taking part in writing and revising the manuscript. Dr AmeraNarey: take part in literature surveying and data interpretation.

Conflicts of interest

The authors of this manuscript are confirming that they have no conflict of interests with any organization or any person.

Acknowledgements

The authors extend their appreciation to the Deanship of Scientific Research at King Khalid University for funding this work through Large Groups (R.G.P. 2/8/44)

References

1 A. Saravanan, P. S. Kumar, S. Jeevanantham, S. Karishma, B. Tajsabreen, P. R. Yaashikaa and B. Reshma, Effective water/wastewater treatment methodologies for toxic pollutants removal: Processes and applications towards sustainable development, *Chemosphere*, 2021, **280**, 130595.

2 W. S. Chai, J. Y. Cheun, P. S. Kumar, M. Mubashir, Z. Majeed, F. Banat, *et al*, A review on conventional and novel materials towards heavy metal adsorption in wastewater treatment application, *J. Cleaner Prod.*, 2021, **296**, 126589.

3 C. Bhattacharjee, S. Dutta and V. K. Saxena, A review on biosorptive removal of dyes and heavy metals from wastewater using watermelon rind as absorbent, *Environ. Adv.*, 2020, **2**, 1–13.

4 B. S. Rathi, P. S. Kumar and P. L. Show, A review on effective removal of emerging contaminants from aquatic systems: Current trends and scope for further research, *J. Hazard. Mater.*, 2021, **409**, 124413.

5 W. S. Chai, J. Y. Cheun, P. S. Kumar, M. Mubashir, Z. Majeed, F. Banat, S.-H. Ho and P. L. Show, A review on conventional and novel materials towards heavy metal adsorption in wastewater treatment application, *J. Cleaner Prod.*, 2021, **296**, 126589.

6 M. Bilal, I. Ihsanullah, M. Younas and M. U. H. Shah, Recent advances in applications of low-cost adsorbents for the removal of heavy metals from water: A critical review, *Sep. Purif. Technol.*, 2021, **278**, 119510.

7 M. Naushad, A. A. Alqadami, Z. A. AlOthman, I. H. Alsohaimi, M. S. Algamdi and A. M. Aldawsari, Adsorption kinetics, isotherm and reusability studies for the removal of cationic dye from aqueous medium using arginine modified activated carbon, *J. Mol. Liq.*, 2019, **293**, 111442.

8 C. Arora, S. Soni, S. Sahu, J. Mittal, P. Kumar and P. Bajpai, Iron-based metal organic framework for efficient removal of methylene blue dye from industrial waste, *J. Mol. Liq.*, 2019, **284**, 343–352.

9 A. Bakry, M. S. Darwish and T. F. Hassanein, Adsorption of methylene blue from aqueous solutions using carboxyl/nitro-functionalized microparticles derived from polypropylene waste, Iran, *Polym. J.*, 2022, 1–13.

10 S. Jafarinejad, Forward osmosis membrane technology for nutrient removal/recovery from wastewater: Recent advances, proposed designs, and future directions, *Chemosphere*, 2021, **263**, 128116.

11 S. Ihaddaden, D. Aberkane, A. Boukerroui and D. Robert, Removal of methylene blue (basic dye) by coagulation-flocculation with biomaterials (bentonite and Opuntiaficusindica), *J. Water Process. Eng.*, 2022, **49**, 102952.

12 A. M. Masoud, M. F. Kamel, M. H. Taha and A. A. El-Zahhar, Phosphonates-based chelating materials for optimization iron removal from industrial wastewater: experimental methodology and modeling, *Fresenius Environ. Bull.*, 2022, **31**(3), 2779–2789.

13 M. H. Taha, A. M. Masoud, Y. M. Khawassek, A. E. Hussein, H. F. Aly and E. Guibal, Cadmium and iron removal from phosphoric acid using commercial resins for purification purpose, *Environ. Sci. Pollut. Res.*, 2020, **27**, 31278–31288.

14 P. Jia, H. Tan, K. Liu and W. Gao, Removal of methylene blue from aqueous solution by bone char, *Appl. Sci.*, 2018, **8**(10), 1903.

15 H. Radnia, A. A. Ghoreyshi, H. Younesi and G. D. Najafpour, Adsorption of Fe (II) ions from the aqueous phase by chitosan adsorbent: equilibrium, kinetic, and thermodynamic studies, *Desalin. Water Treat.*, 2012, **50**(1–3), 348–359.

16 L. L. Sui, H. Zhang, H. Ren and H. B. Xu, Adsorption of Fe (II) Ions from Aqueous Solution Using Silica-Supported Organic–Inorganic Hybrid Sorbents, *Russ. J. Phys. Chem. A*, 2019, **93**, 936–945.

17 A. A. Elzoghby, A. Bakry, A. M. Masoud, W. S. Mohamed, M. H. Taha and T. F. Hassanein, Synthesis of polyamide-based nanocomposites using green-synthesized chromium and copper oxides nanoparticles for the sorption of uranium from aqueous solution, *J. Environ. Chem. Eng.*, 2021, **9**(6), 106755.

18 W. W. Ngah, S. Ab Ghani and A. Kamari, Adsorption behavior of Fe (II) and Fe (III) ions in aqueous solution on chitosan and cross-linked chitosan beads, *Bioresour. Technol.*, 2005, **96**(4), 443–450.

19 A. R. Kaveeshwar, S. K. Ponnusamy, E. D. Revellame, D. D. Gang, M. E. Zappi and R. Subramaniam, Pecan shell-based activated carbon for removal of iron (II) from fracking wastewater: adsorption kinetics, isotherm, and thermodynamic studies, *Process Saf. Environ. Prot.*, 2018, **114**, 107–122.

20 Y. Guesmi, H. Agougui, R. Lafi, M. Jabli and A. Hafiane, Synthesis of hydroxyapatite-sodium alginate via a co-precipitation technique for efficient adsorption of Methylene Blue dye, *J. Mol. Liq.*, 2018, **249**, 912–920.

21 J. Bu, L. Yuan, N. Zhang, D. Liu, Y. Meng and X. Peng, High-efficiency adsorption of methylene blue dye from wastewater by a thiosemicarbazide functionalized graphene oxide composite, *Diamond Relat. Mater.*, 2020, **101**, 107604.

22 A. Bakry, M. S. Darwish and A. M. A. El Naggar, Assembling of hydrophilic and cytocompatible three-dimensional scaffolds based on aminolyzed poly (L-lactide) single crystals, *New J. Chem.*, 2018, **42**(20), 16930–16939.

23 R. S. Mohamed, A. A. Al Kahlawy, A. M. A. El Naggar and H. M. Gobara, Innovative approach for production of carbon nanotubes (CNT_S) and carbon nano-sheets through highly efficient photocatalytic water splitting into hydrogen using metal organic frameworks (MOF)-nano TiO_2 matrix as novel catalyst, *New J. Chem.*, 2020, **44**, 5097–5108.

24 A. M. A. El Naggar, A. G. Soliman, M. R. Noor El-Din, A. M. Ramadan and M. A. Youssef, Synthesis of porous of poly-HIPE @ nano silica core-shell composites and their application for oily wastewater treatment, *J. Polym. Res.*, 2022, **29**(2), 35.

25 A. Saravanan, P. Thamarai, P. S. Kumar and G. Rangasamy, Recent advances in polymer composite, extraction, and

their application for wastewater treatment: A review, *Chemosphere*, 2022, 136368.

26 G. Sarojini, S. V. Babu, N. Rajamohan, M. Rajasimman and A. Pugazhendhi, Application of a polymer-magnetic-algae based nano-composite for the removal of methylene blue–characterization, parametric and kinetic studies, *Environ. Pollut.*, 2022, **292**, 118376.

27 A. S. A. Bakr, H. Al-Shafey, E. I. Arafa and A. M. A. El Naggar, Synthesis and characterization of polymerized acrylamide coupled with acrylamido-2-Methyl-1-propane sulfonic acid-montmorillonite structure as a novel nanocomposite for Cd (II) removal from aqueous solutions, *J. Chem. Eng. Data*, 2020, **65**(8), 4079–4091.

28 H. Han, M. K. Rafiq, T. Zhou, R. Xu, O. Mašek and X. Li, A critical review of clay-based composites with enhanced adsorption performance for metal and organic pollutants, *J. Hazard. Mater.*, 2019, **369**, 780–796.

29 M. Safarpour, S. Arefi-Oskoui and A. Khataee, A review on two-dimensional metal oxide and metal hydroxide nanosheets for modification of polymeric membranes, *J. Ind. Eng. Chem.*, 2020, **82**, 31–41.

30 F. Lakhal, A. Maghchiche, R. Nasri and A. Haouam, Composite material polystyrene activated carbon for water purification, *J. Mater. Environ. Sci.*, 2018, **9**(8), 2411–2417.

31 Q. Zhang, Q. Du, M. Hua, T. Jiao, F. Gao and B. Pan, Sorption enhancement of lead ions from water by surface charged polystyrene-supported nano-zirconium oxide composites, *Environ. Sci. Technol.*, 2013, **47**(12), 6536–6544.

32 R. Kumar, Fabrication of Polystyrene/AlOOH Hybrid Material for Pb (II) Decontamination from Wastewater: Isotherm, Kinetic, and Thermodynamic Studies, *Colloids Interfaces*, 2022, **6**(4), 72.

33 Y. Chen, S. Chen, Z. Deng, X. Xu, J. Qin, X. Guo, Z. Bai, X. Chen and Z. Lu, Fabrication of polystyrene/CuO@ calcined layered double hydroxide microspheres with high adsorption capacity for Congo red, *Colloids Surf., A*, 2022, **652**, 129827.

34 L. Mohammadi, A. Rahdar, R. Khaksefidi, A. Ghamkhari, G. Fytianos and G. Z. Kyzas, Polystyrene magnetic nanocomposites as antibiotic adsorbents, *Polym*, 2020, **12**(6), 1313.

35 M. M. A. Khan, Preparation, characterization, biological activity, and transport study of polystyrene-based calcium–barium phosphate composite membrane, *Mater. Sci. Eng., C*, 2013, **33**(7), 4228–4235.

36 A. M. Youssef, F. M. Malhat and A. F. A. Abd El-Hakim, Preparation and utilization of polystyrene nanocomposites based on TiO2 nanowires, *Polym.-Plast. Technol. Eng.*, 2013, **52**(3), 228–235.

37 D. Goswami and H. Kalita, Rapid determination of iron in water by modified thiocyanate method, *Def. Sci. J.*, 1988, **38**(2), 177–182.

38 J. Loste, J.-M. Lopez-Cuesta, L. Billon, H. Garay and M. Save, Transparent polymer nanocomposites: An overview on their synthesis and advanced properties, *Prog. Polym. Sci.*, 2019, **89**, 133–158.

39 A. Ansari and M. J. Akhtar, Investigation on electromagnetic characteristics, microwave absorption, thermal and mechanical properties of ferromagnetic cobalt–polystyrene composites in the X-band (8.4–12.4 GHz), *RSC Adv.*, 2016, **6**(17), 13846–13857.

40 H.-J. Kang and J.-H. Kim, Adsorption kinetics, mechanism, isotherm, and thermodynamic analysis of paclitaxel from extracts of Taxuschinensis cell cultures onto Sylopute, *Biotechnol. Bioprocess Eng.*, 2019, **24**, 513–521.

41 M. H. Taha, S. A. Abdel Maksoud, M. M. Ali, A. M. A. El Naggar, A. S. Morshedy and A. A. Elzoghby, Conversion of biomass residual to acid-modified bio-chars for efficient adsorption of organic pollutants from industrial phosphoric acid: an experimental, kinetic and thermodynamic study, *Int. J. Environ. Anal. Chem.*, 2019, **99**(12), 1211–1234.

42 A. F. Abou-Hadid, U. A. El-Behairy, M. M. Elmalih, E. Amdeha, A. M. El Naggar, M. H. Taha and A. E. Hussein, Production of efficient carbon fiber from different solid waste residuals for adsorption of hazardous metals from wastewater samples, *Biomass Convers. Biorefin.*, 2022, 1–16.

43 K. Y. Foo and B. H. Hameed, Insights into the modeling of adsorption isotherm systems, *Chem. Eng. J.*, 2010, **156**(1), 2–10.

44 K. He, G. Zeng, A. Chen, Z. Huang, M. Peng, T. Huang and G. Chen, Graphene hybridized polydopamine-kaolin composite as an effective adsorbent for methylene blue removal, *Composites, Part B*, 2019, **161**, 141–149.

45 H. Gomaa, E. M. Abd El-Monaem, A. S. Eltaweil and A. M. Omer, Efficient removal of noxious methylene blue and crystal violet dyes at neutral conditions by reusable montmorillonite/NiFe2O4@ amine-functionalized chitosan composite, *Sci. Rep.*, 2022, **12**(1), 15499.

46 F. Aeenjan and V. Javanbakht, Methylene blue removal from aqueous solution by magnetic clinoptilolite/chitosan/EDTA nanocomposite, *Res. Chem. Intermed.*, 2018, **44**, 1459–1483.

47 C. Dai, M. Zhang, X. Guo and X. Ma, Mesoporous composite Ni-CN/SA for selective adsorption of methylene blue from water, *Chem. Eng. J.*, 2021, **407**, 127181.

48 S. Wu, J. Huang, C. Zhuo, F. Zhang, W. Sheng and M. Zhu, One-step fabrication of magnetic carbon nanocomposite as adsorbent for removal of methylene blue, *J. Inorg. Organomet. Polym. Mater.*, 2016, **26**, 632–639.

49 Y. Zhang, J. Zhao, Z. Jiang, D. Shan and Y. Lu, Biosorption of Fe (II) and Mn (II) ions from aqueous solution by rice husk ash, *BioMed Res. Int.*, 2014, **2014**, 973095.

50 N. A. Reiad, O. E. A. Salam, E. F. Abadir and F. A. Harraz, Adsorptive removal of iron and manganese ions from aqueous solutions with microporous chitosan/polyethylene glycol blend membrane, *J. Environ. Sci.*, 2012, **24**(8), 1425–1432.

51 J. C. Moreno-Piraján, V. S. Garcia-Cuello and L. Giraldo, The removal and kinetic study of Mn, Fe, Ni and Cu ions from wastewater onto activated carbon from coconut shells, *Adsorption*, 2011, **17**, 505–514.

52 E. Daneshvar, A. Vazirzadeh, A. Niazi, M. Kousha, M. Naushad and A. Bhatnagar, Desorption of methylene blue dye from brown macroalga: effects of operating parameters, isotherm study, and kinetic modeling, *J. Cleaner Prod.*, 2017, **152**, 443–453.

53 S. Madhavakrishnan, K. Manickavasagam, Y. Sameena, K. Selvam, K. KairveluK and S. Pattabhi, Adsorption of Iron (II) from Aqueous Solution Using Ricinuscommunis Pericarp Carbon as an Adsorbent, *Nat., Environ. Pollut. Technol.*, 2006, **115**, 58–97.

54 H. Gomaa, E. M. Abd El-Monaem, A. S. Eltaweil and A. M. Omer, Efficient removal of noxious methylene blue and crystal violet dyes at neutral conditions by reusable montmorillonite/NiFe2O4@ amine-functionalized chitosan composite, *Sci. Rep.*, 2022, **12**(1), 15499.

55 K. T. Kubra, M. S. Salman, H. Znad and M. N. Hasan, Efficient encapsulation of toxic dye from wastewater using biodegradable polymeric adsorbent, *J. Mol. Liq.*, 2021, **329**, 115541.